New Journal of Physics
The open access journal at the forefront of physics

Deutsche Physikalische Gesellschaft DPG
IOP Institute of Physics

Published in partnership with: Deutsche Physikalische Gesellschaft and the Institute of Physics

OPEN ACCESS

RECEIVED
7 August 2014

REVISED
25 December 2014

ACCEPTED FOR PUBLICATION
2 January 2015

PUBLISHED
4 February 2015

PAPER

Laser acceleration of protons using multi-ion plasma gaseous targets

Tung-Chang Liu[1], Xi Shao[1], Chuan-Sheng Liu[1], Bengt Eliasson[1,2], W T Hill III[1], Jyhpyng Wang[3,4] and Shih-Hung Chen[4]

[1] Department of Physics, University of Maryland, College Park, Maryland 20742, USA
[2] SUPA, Department of Physics, Strathclyde University, Glasgow G4 0NG, United Kingdom
[3] Institute of Atomic and Molecular Sciences, Academia Sinica, Taipei 10617, Taiwan
[4] Department of Physics, National Central University, Taoyuan 32001, Taiwan

E-mail: tcliu@umd.edu

Keywords: laser–plasma acceleration of electrons and ions, particle-in-cell method, laser–plasma interactions, relativistic plasmas

Abstract

We present a theoretical and numerical study of a novel acceleration scheme by applying a combination of laser radiation pressure and shielded Coulomb repulsion in laser acceleration of protons in multi-species gaseous targets. By using a circularly polarized CO_2 laser pulse with a wavelength of 10 μm—much greater than that of a Ti: Sapphire laser—the critical density is significantly reduced, and a high-pressure gaseous target can be used to achieve an overdense plasma. This gives us a larger degree of freedom in selecting the target compounds or mixtures, as well as their density and thickness profiles. By impinging such a laser beam on a carbon–hydrogen target, the gaseous target is first compressed and accelerated by radiation pressure until the electron layer disrupts, after which the protons are further accelerated by the electron-shielded carbon ion layer. An 80 MeV quasi-monoenergetic proton beam can be generated using a half-sine shaped laser beam with a peak power of 70 TW and a pulse duration of 150 wave periods.

1. Introduction

The laser acceleration of quasi-monoenergetic protons has recently drawn tremendous interest due to its potential applications in cancer treatment [1, 2], proton radiography [3], and isotope production for positron emission tomography [4]. In the realm of laser acceleration of protons from a target foil, there are mainly two schemes being widely studied: target normal sheath acceleration [5–14] (TNSA) and radiation pressure acceleration (RPA). In particular, to acquire quasi-monoenergetic protons, the scheme of laser RPA has been actively studied in theory and simulations [15–23] and experiments [24–26]. In RPA in the light-sail region, a high intensity laser beam irradiates an overdense thin foil (or an overdense thin foil formed by laser radiation compression) and accelerates nearly the whole foil. The electrons are trapped by a combination of the laser ponderomotive force and the electric force due to the ions, and the protons in the accelerating frame are subject to both the electric force of the electron layer accelerating them forward and the inertial force pulling them back. The balance of these opposing forces forms a trap for the proton and electron layers, resulting in a self-organized double layer [21]. Therefore, RPA could potentially produce high-energy monoenergetic protons suitable for many applications, if the accelerated protons have good beam quality and a narrow energy spectrum. However, previous works have demonstrated [20, 22, 25, 27, 28] that the Rayleigh–Taylor instability (RTI) limits the proton energy achieved by RPA and rapidly broadens the proton beam's energy spectrum.

On the other hand, by using multi-species targets, which are now actively studied [26, 29–31], the broadening of the proton energy spectrum due to instabilities could be largely suppressed. By using a thin composite foil made of carbon and hydrogen with a relatively large carbon concentration, we found in our recent work [32] that there are two different stages of acceleration to further push the proton forward. In the initial RPA stage, the heavier carbon ions are left behind the lighter protons, and a triple-layer system of carbon

ions, protons, and electrons is formed. After that, the electron layer has been disrupted by the RTI, and the shielded Coulomb repulsion (SCR) stage takes place, in which the proton layer continues to be pushed forward by the electron-shielded carbon ion layer behind it. The carbon layer delays the disruption of the proton layer by the RTI and further accelerates the protons. Our simulation study showed that, using a 70 terawatt laser beam to irradiate a carbon-proton target with 10% protons, a quasi-monoenergetic proton beam with 60 MeV of energy can be achieved, which is several times the energy obtained from a pure hydrogen foil.

In order to successfully accelerate the protons by the Coulomb repulsion force, we should both reduce the charge difference between carbon ions and electrons and keep the electrons from returning to the carbon layer so that the net charge of the carbon-electron layer is positive. In our previous works [32, 33], we concluded that a higher carbon concentration and smaller spot size can lead to increased proton energy.

One main concern about the laser acceleration of a thin solid target is that ultra-thin solid targets of uniformly mixed 90% carbon and 10% hydrogen, i.e., $C_{0.9}H_{0.1}$ in an empirical formula or other compound foils with a high carbon concentration, are difficult to manufacture [34, 35]. On the other hand, if we use a laser beam with a longer wavelength, then the critical density, which has an inverse quadratic dependence on laser wavelength, will be strongly reduced; therefore, high-pressure gaseous targets can be used in the acceleration scheme. It has been demonstrated, for example, that micrometer-sized nozzles and skimmers can be used to produce supersonic helium atom beams [36]. Previous numerical and experimental studies [23, 37] showed that it is possible to produce high-energy quasi-monoenergetic proton beams from a gaseous hydrogen target accelerated by a CO_2 laser with a wavelength of 10 μm.

There are interesting differences between a thin foil with a thickness smaller than the laser wavelength and a thick gaseous target, besides the fact that a longer wavelength corresponds to lower critical density. A thicker target with a density profile maximized at the center represents a more realistic gas extruded from a nozzle. Moreover, a rich combination acceleration mechanism consists of caviton formation due to the reflected wave, hole-boring, and significant target compression. TNSA and shock could all be observed in the acceleration process, whereas in the laser acceleration of protons using ultrathin solid foil, the acceleration mechanisms involved are mainly only RPA and SCR.

In this paper, we demonstrate by two-dimensional (2D) particle-in-cell (PIC) simulation that a quasi-monoenergetic proton beam can be obtained using a long acceleration time, where the signatures of RPA, SCR, TNSA, and shock acceleration [38, 39] can all be observed. We discuss advantages and disadvantages with different target thicknesses and densities, and then finally compare the proton energy evolution between the simulation results and our theoretical model and show that RPA and SCR are two main effects in the acceleration process.

2. Simulation setup

In order to investigate the acceleration of protons in a multi-ion gaseous target, we employ 2D PIC simulations using VORPAL [40]. The simulation domain is $-50 \leqslant x/\lambda_L \leqslant 100$ and $-25 \leqslant y/\lambda_L \leqslant 25$, and the grid size is $\lambda_L/100$ in the x dimension and $\lambda_L/50$ in the y dimension, where $\lambda_L = 10$ μm is the laser wavelength. The boundary conditions are absorbing at all boundaries for particles and fields, and the laser wave is injected at the negative x −boundary. The amplitude of the incident laser has a Gaussian profile in the transverse direction with waist size $w_0 = 4.0\lambda_L$, defined as the diameter $d = 2w_0$ at e^{-2} of the peak intensity, a half-sine wave in the time profile with normalized peak amplitude $a_0 = eE_{y,z}/m_e\omega_L c = 10$, and a full duration of $\tau_L = 150T_L$, as shown in figure 1(a), where $T_L = \lambda_L/c_0$ is the laser wave period. The pre-ionized target, shown in figures 1(b) and (c), consists of 90% carbon and 10% hydrogen and is initially located at $0 \leqslant x \leqslant l_0$ with the initial thickness $l_0 = 2.5\lambda_L$ and the electron density profile

$$n_{e0}(x) = n_{e0\,max} \exp\left[-\left(\frac{x - l_0/2}{l_0/4}\right)^2\right] \quad (1)$$

with $n_{e0\,max} = 6n_{C^{6+}0\,max} + n_{p^+0\,max} = 10n_{cr}$ and $n_{C^{6+}0\,max}$: $n_{p^+0\,max} = 9{:}1$. Here, pre-ionized carbon is allocated as a representative of a heavy ion and could be replaced by any gaseous molecule with its nucleus having the same charge-to-mass ratio, such as helium or nitrogen. The target is resolved by 49 macro-particles per cell at the density maximum for all species. Here $n_{cr} = \varepsilon_0 m_e \omega_L^2/e^2$ is the critical density, where m_e is the electron mass, e is the elementary charge, ε_0 is the electric vacuum permittivity, and ω_L is the laser angular frequency. We define $t = 0$ as the time when the laser beam starts to interact with the target.

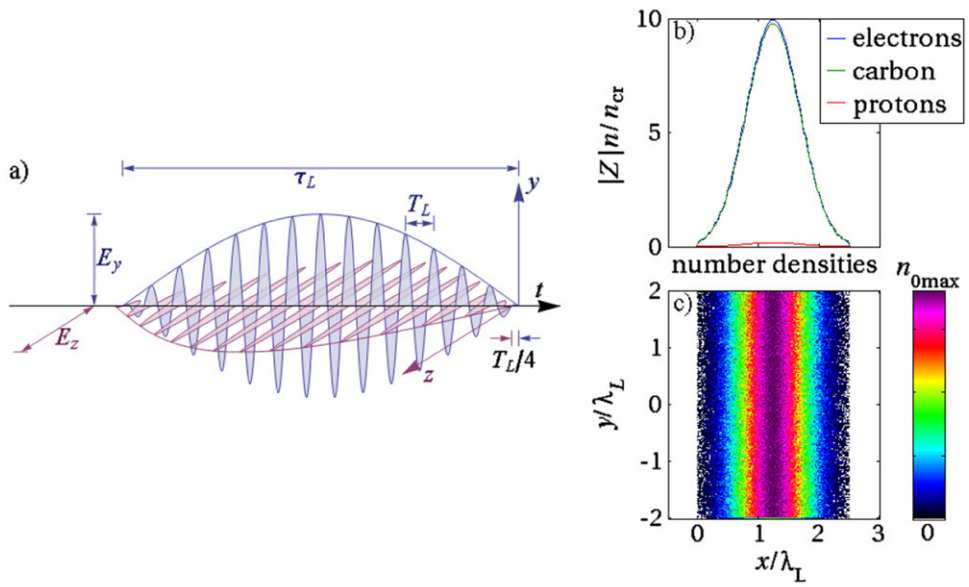

Figure 1. The initial setup of (a) the laser beam and (b), (c) the particle densities in the target. The window is enlarged around the center of the target.

3. Simulation result and analysis

We compare the phase space and density distributions at different times and analyze the acceleration mechanisms individually. Figures 2 and 3 show the phase space and number density distributions of carbon ions and electrons, whereas figure 3 shows the enlargements of figures 2(l) and (g), and figure 4 shows those of protons. Here the y-axes of the phase space distributions are in normalized units $p_x/mc = \gamma\beta_x$, where p_x is the momentum of particle in the longitudinal direction, m is the mass of the particle, $\beta_x = v_x/c$ is the normalized longitudinal velocity, and $\gamma = (1 - \beta_x^2 - \beta_y^2 - \beta_z^2)^{-1/2}$ is the gamma factor of the particle. The time evolution of the proton energy spectrum is shown in figure 5. First, at $20T_L$ after the interaction starts between the laser beam and the gaseous target, the laser beam compresses the electrons and forms a caviton at critical density, as shown in figure 2(a). The compressed electron layer then pulls the ions forward, forming a self-induced double layer, or so-called light sail. Figure 4(a) shows that a small portion of protons are accelerated by the highly compressed overdense mirror and move almost twice as fast as the radiation pressure-accelerated light sail. At $t = 40T_L$, when the intensity of the pulse continues to increase, almost all particles of the target are highly compressed and accelerated, as shown in figures 2(q) and 4(l). On the other hand, the RTI becomes observable in the density distributions of all the particles (figures 2(b), (g), and 4(g)), indicating the decomposition of the electron-carbon target and the decrease of their densities. In their phase spaces (figures 2(l) and 4(b)), we could observe all the features of RPA, shock, and TNSA along the acceleration processes of carbon ions and protons, as indicated in figure 2(l). The enlargement of the carbon phase space and density distribution (figure 3) shows a clear signature of RPA, which compresses and accelerates the plasma at a layer located at $x \approx 1.4\lambda_L$. It also shows shock acceleration of the carbon ions with the layer having a similar shape as the RPA accelerated one at $x \approx 1.8\lambda_L$ by the large shock potential, as well as TNSA by the electron sheath in front of the carbon layer, pulling the ion in the front side forward. There is also a left-behind tail of protons becoming untrapped and moving backward $\left(\gamma\beta_x < 0\right)$ due to the Coulomb repulsion during the acceleration. That is, there is a small number of protons that is backward accelerated.

At $t = 70T_L$, the injected laser amplitude is near its peak $a_0 = 10$ at the target. The density of electrons, however, is relativistically underdense to the laser wave, since $n_{e,\max} \sim 2n_{cr} < 10n_{cr}$, as shown in figure 2(r). The laser starts to penetrate the electron cloud, and the thermal expansion of the electrons and carbon ions becomes more and more significant. As a result, all carbon ions that accelerated due to the acceleration mechanisms of shock, RPA, and TNSA, as mentioned previously, start to merge altogether (figures 2(m) and 4(c)). Meanwhile, because of a greater charge-to-mass ratio, some of the protons are further accelerated, leaving some of them trapped in the carbon ion layer and a small amount of them being accelerated in a backward direction. The front end, as well as the rear end, of the proton layer start to be accelerated by the SCR in both directions at this time.

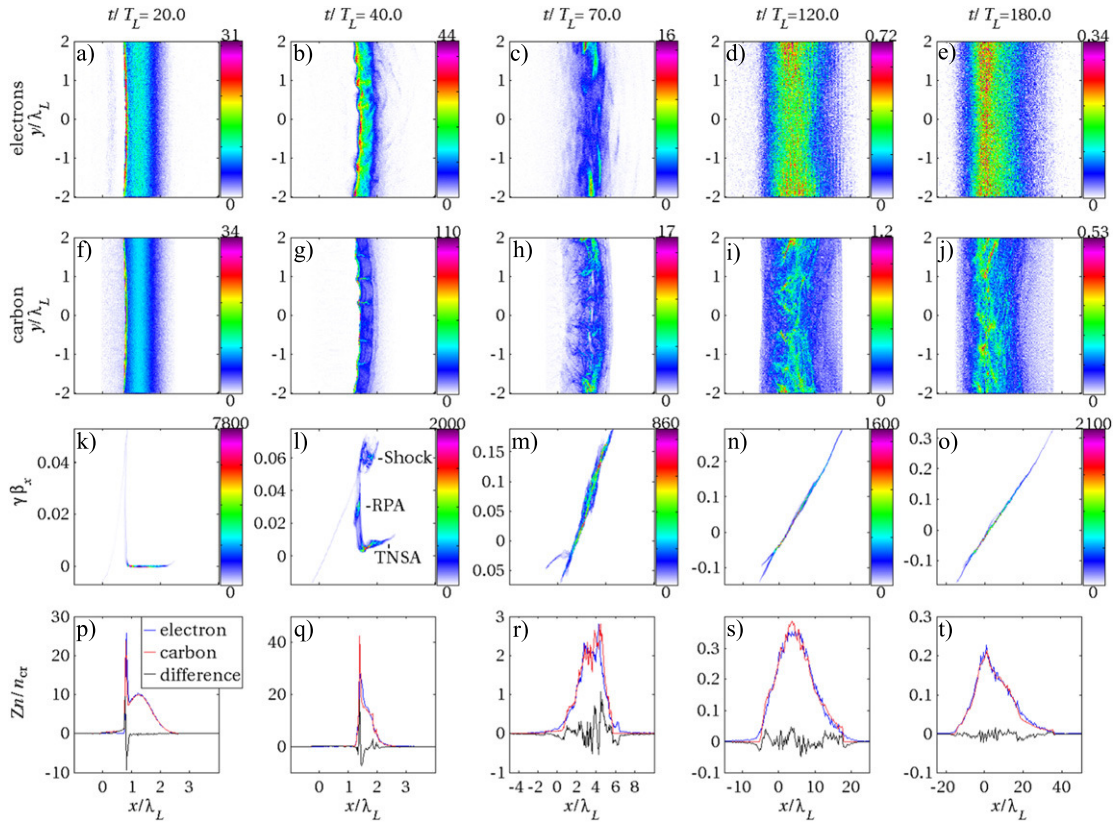

Figure 2. Two-dimensional density distributions of electrons (1st row) and carbon ions (2nd row), the carbon ion phase space (3rd row), and the one-dimensional density distribution (4th row) of electrons, carbon ions, and their differences, which are plotted by averaging over $-0.5\lambda_L < y < 0.5\lambda_L$, at times $t = 20T_L$, $40T_L$, $70T_L$, $120T_L$ and $180T_L$.

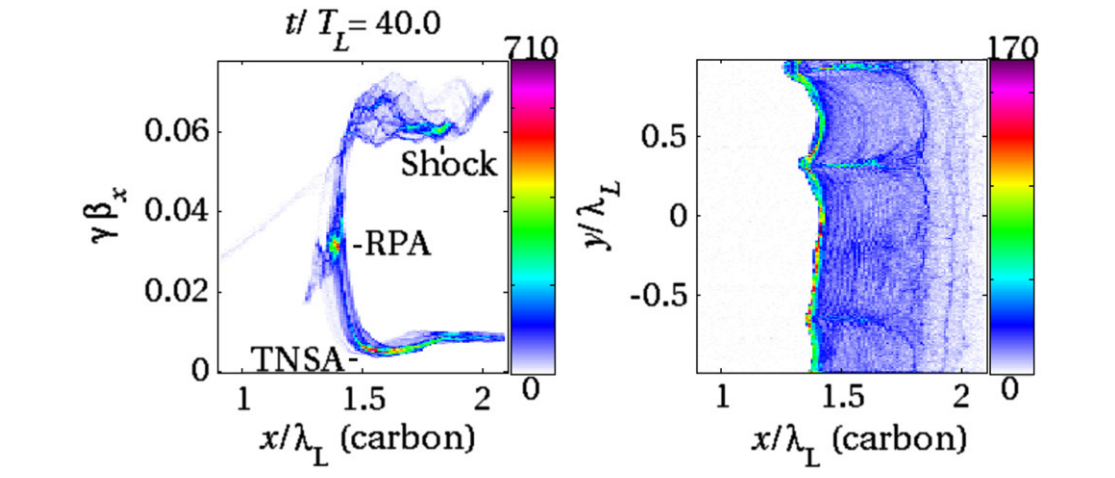

Figure 3. An enlargement of phase and density distribution of the carbon ion at $t = 40T_L$.

At $t = 120T_L$, the intensity of the laser pulse is decreasing, and the phase space of carbon ions shown in figure 2(n) illustrates that almost all of the carbon ions are merged into a straight line. This means that they are no longer being affected by the laser beam while the electrons are trapped by the Coulomb potential of the carbon ions. The protons at this time (the fourth column of figure 4) are separated into three distinct parts—the ones that stay in front of and behind the carbon ions, pushed bi-directionally by the SCR, and the ones trapped in the carbon ions. Since the repulsion force decreases with increasing distance, the protons left behind are more accelerated. As a result, the velocity difference could be reduced, and the proton layer becomes more monoenergetic (figures 4(d) and 5).

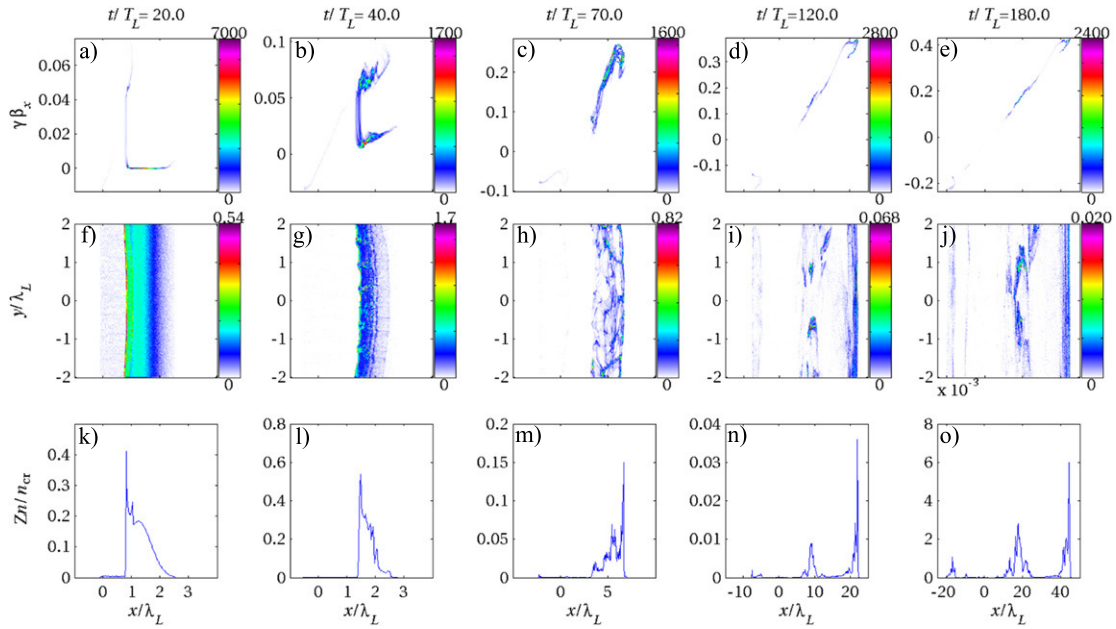

Figure 4. The phase space (1st row), two-dimensional density distribution (2nd row), and one-dimensional density distribution (3rd row) of protons, plotted by averaging over $-0.5\lambda_L < y < 0.5\lambda_L$, at times $t = 20T_L$, $40T_L$, $70T_L$, $120T_L$ and $180T_L$.

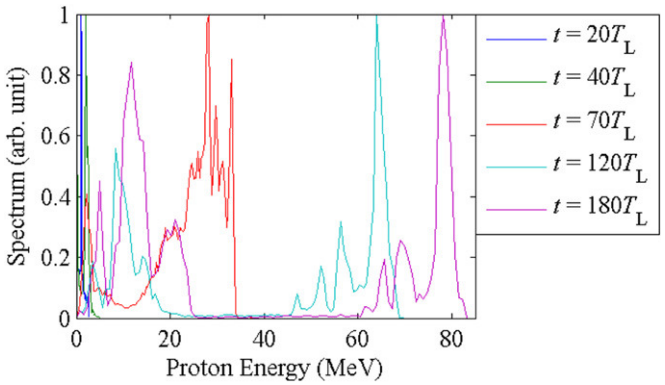

Figure 5. The proton energy spectra at different times within $|y| < \lambda_L$.

Finally, when the laser pulse has completely left the target, the carbon ions expand freely, and the electrons follow the density profile of the carbon ions, as shown in the last column of figure 2. Figure 4(e) shows that the protons continue to be accelerated by SCR without losing the monoenergetic property, indicating that this SCR can stably accelerate the protons for a long time. Figure 5 shows a distinct peak at the proton energy 80 MeV at time $t = 180T_L$.

4. Targets with larger density or thickness

The question of whether increasing the target density or thickness could further increase the energy of quasi-monoenergetic protons is of interest. Since the number of particles being accelerated is increased, the energy conversion efficiency could increase if the energy and the number of the protons in the monoenergetic peak do not drop too significantly. Therefore, in this section, simulations with the same laser parameters, but using targets with larger density or thickness, are performed.

We first investigate the case with doubled target thickness and with other parameters remaining unchanged. Figure 6 shows the comparison of the proton profiles of the original case and the case with doubled thickness. In the case with doubled thickness, the proton layer is not compressed to form a quasi-monoenergetic layer. Therefore, we conclude that there exists an upper limit of target thickness l_{lim} for the proton layer to be successfully compressed into and remain as one quasi-monoenergetic layer. In our laser parameters with a

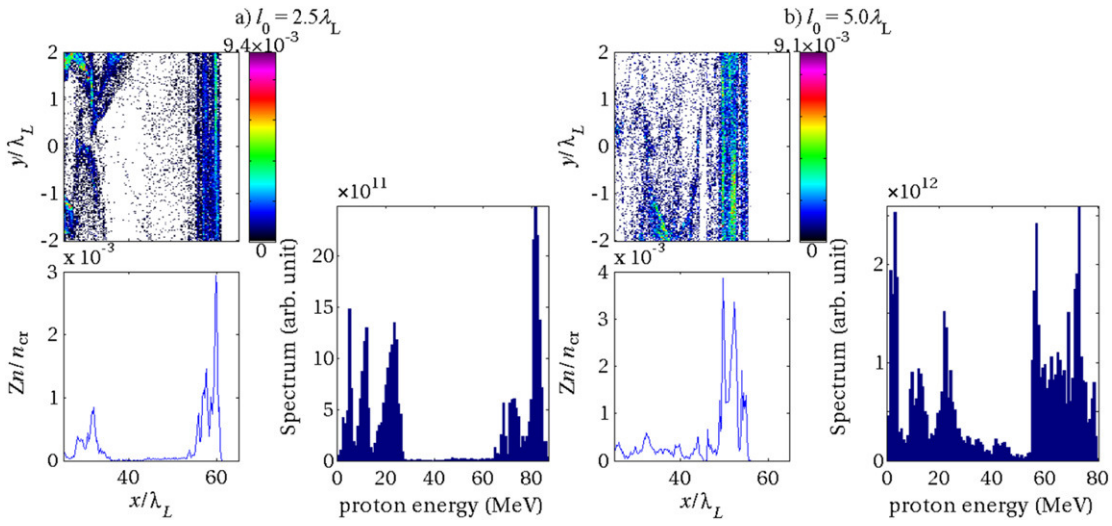

Figure 6. The comparison of two-dimensional density distributions and one-dimensional density distributions by averaging over $-0.5\lambda_L < y < 0.5\lambda_L$, and energy spectra of the protons within $|y| < \lambda_L$ at $t = 220T_L$ between (a) the original case of $l_0 = 2.5\lambda_L$ and (b) the case with doubled thickness $l_l = 5.0\lambda_L$.

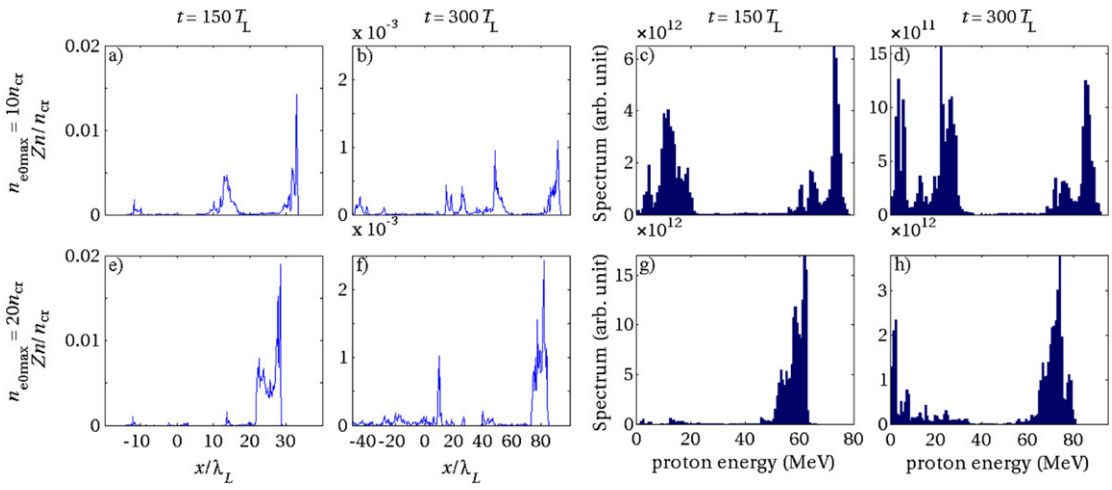

Figure 7. The one-dimensional density distributions (the first two columns) and energy spectra (the last two columns) of protons within $|y| < \lambda_L$ at $t = 150T_L$ and $t = 300T_L$ between the original case of $n_{e0\,max} = 10n_{cr}$ (the 1st row) and the case with doubled peak density $n_{e0\,max} = 20n_{cr}$ (the 2nd row).

density peak of $n_{e0\,max} = 10n_{cr}$, we have $l_{lim} < 5.0\lambda_L = 50\mu$m. In comparison, the optimal thickness of RPA with single species foil [16, 19] is $l_{opt}/\lambda_L = \left(a_0/\pi\right)\Big/\left(n_{e0}/n_{cr}\right) \approx 0.6$, much smaller than this limiting value.

On the other hand, the result is quite different for the case with doubled peak density, although the surface density is the same as in the doubled-thickness case. The target with doubled density could be viewed as being compressed by a factor of two from the doubled-thickness case. Therefore, it reduces the time and energy the laser spends in compression. The comparison shown in figure 7 indicates that the case with doubled initial peak density could trap about two times more protons in the front layer and remain quasi-monoenergetic during the acceleration. However, due to the increased target mass, the acceleration is slightly lower than for the original case. Therefore, doubling the target peak density could result in an overall increase in the energy conversion efficiency with a larger number of protons but with lower energy.

5. Discussion

In this section, we calculate the evolution of the proton momentum, using equations of motion of RPA and SCR, and compare them with the simulation of the original and double-peak-density cases. The equations of motion

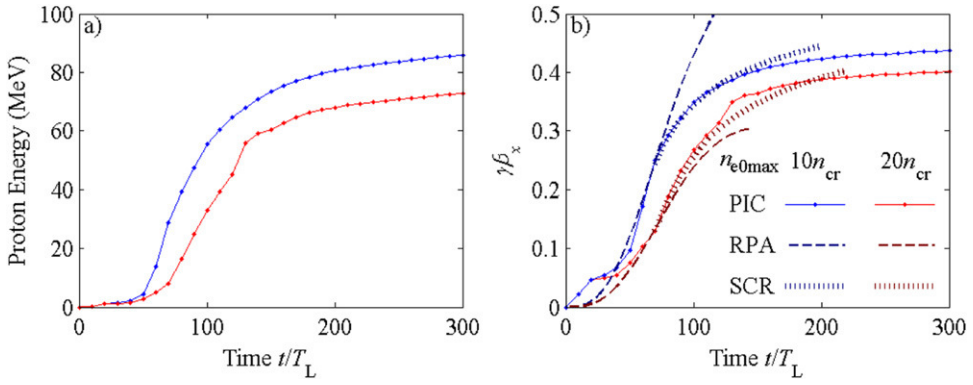

Figure 8. The evolutions of proton (a) energy and (b) momentum. Theoretical predictions of RPA and SCR are shown in panel (b).

of RPA can be written as [19]

$$\begin{cases} \dfrac{\mathrm{d}x_\mathrm{i}}{\mathrm{d}t} = \beta_\mathrm{i} \\ \dfrac{\mathrm{d}\gamma_\mathrm{i}\beta_\mathrm{i}}{\mathrm{d}\left(t/T_\mathrm{L}\right)} = 2\dfrac{m_\mathrm{e}}{m_\mathrm{i}}\dfrac{n_\mathrm{cr}}{n_0}\dfrac{\lambda_\mathrm{L}}{l_0}a\left(x_\mathrm{i},\, t\right)^2\dfrac{1-\beta_\mathrm{i}}{1+\beta_\mathrm{i}}, \end{cases} \tag{2}$$

where

$$a\left(x_\mathrm{i},\, t\right) = a_0 \sin\left[-\frac{\pi}{\tau_\mathrm{L}}\left(\frac{x_\mathrm{i}}{\lambda_\mathrm{L}} - \frac{t}{T_\mathrm{L}}\right)\right], \quad -\tau_\mathrm{L} < \frac{x_\mathrm{i}}{\lambda_\mathrm{L}} - \frac{t}{T_\mathrm{L}} < 0 \tag{3}$$

is the instantaneous normalized amplitude of the laser at the target, with $\tau_\mathrm{L} = t_\mathrm{L}/T_\mathrm{L} = 150$ being the normalized laser pulse length. The subscript 'i' stands for ions, a combination of carbon ions and protons. Figure 8(b) shows that the momentum evolution calculated theoretically generally agrees with the simulation result for $t < 80T_\mathrm{L}$, the acceleration period when the target is overdense. Therefore, RPA is the dominant acceleration mechanism during the first 80 laser periods.

After that, the electron layer has become transparent, and the Coulomb repulsion continues to moderately accelerate the protons ahead while keeping the quasi-monoenergetic property. The equation of motion of one-dimensional (1D) SCR with the protons assumed to be test charges and the carbon layer moving with constant velocity can be expressed as [32]

$$\begin{cases} \dfrac{\mathrm{d}x_\mathrm{p}}{\mathrm{d}t} = v_\mathrm{p} \\ \dfrac{\mathrm{d}\left(\gamma_\mathrm{p}v_\mathrm{p}\right)}{\mathrm{d}t} = \dfrac{eE_x}{m_\mathrm{p}} = \dfrac{e\sigma_\mathrm{net}}{2\varepsilon_0 m_\mathrm{p}}\coth\dfrac{\left(x_\mathrm{p} - v_C t\right)e\sigma_\mathrm{net}}{4\varepsilon_0 k_\mathrm{B} T_\mathrm{e}}, \end{cases} \tag{4}$$

where σ_net is the net surface charge density of the carbon and electron layer and T_e is the electron temperature. The initial time is set as $t_0 = 70T_\mathrm{L}$, and the initial conditions $(v_{\mathrm{p}0},\ x_{\mathrm{p}0},\ v_{C,}\sigma_\mathrm{net})$ at this time are read from the simulation data. Here we assign $T_\mathrm{e} = 20m_\mathrm{e}c^2$ as a fitting parameter. The theoretical curves shown in figure 8(b) generally agree with the simulation results for an additional time period of $\sim 100T_\mathrm{L}$ and start to over-estimate the energy, while the separation of the carbon and proton layers becomes too large to apply the nearly 1D assumption, where it is assumed that the separation is small compared with the laser spot size. However, since the proton acceleration at that time is almost negligible, and the energy here is nearly a constant (figure 8(a)), the theoretical estimation here is enough to approximate the energy of the proton beam.

6. Conclusions

We have shown that a combination of a series of acceleration mechanisms could be observed in laser acceleration of a gaseous target, where RPA and SCR are the two dominant mechanisms in both accelerating and

stabilizing the proton layer. We have also demonstrated that the quasi-monoenergetic property depends significantly on the compression of the target in the early stages and, consequently, verified that there exists an upper bound less than 50 μm in target thickness in our simulation. We also provided a set of models interpreting the acceleration mechanism and showed that the energy evolution of the proton layer fits well with the theoretical prediction before it undergoes nearly constant velocity motion. It was shown that a quasi-monoenergetic proton beam of energy 80 MeV could be obtained by a CO_2 laser beam of peak power 70 TW and pulse length $150T_L$.

Acknowledgments

This work was supported by US DOE grant DE-SC0008391. We acknowledge the National Center for High-Performance Computing for providing resources under the national project 'Taiwan Knowledge Innovation National Grid'.

References

[1] Jones B 2005 Radiotherapy for the future *BMJ* **330** 979–80
[2] Ledingham K W D, Galster W and Sauerbrey R 2007 Laser-driven proton oncology—a unique new cancer therapy? *Br. J. Radiol.* **80** 855–8
[3] Roth M *et al* 2002 Energetic ions generated by laser pulses: a detailed study on target properties *Phys. Rev. Spec. Top.—Accel. Beams* **5** 061301
[4] Lefebvre E, d' Humières E, Fritzler S and Malka V 2006 Numerical simulation of isotope production for positron emission tomography with laser-accelerated ions *J. Appl. Phys.* **100** 113308
[5] Wilks S C, Langdon A B, Cowan T E, Roth M, Singh M, Hatchett S, Key M H, Pennington D, MacKinnon A and Snavely R A 2001 Energetic proton generation in ultra-intense laser–solid interactions *Phys. Plasmas* **8** 542–9
[6] Pukhov A 2001 Three-dimensional simulations of ion acceleration from a foil irradiated by a short-pulse laser *Phys. Rev. Lett.* **86** 3562–5
[7] Schwoerer H, Pfotenhauer S, Jäckel O, Amthor K-U, Liesfeld B, Ziegler W, Sauerbrey R, Ledingham K W D and Esirkepov T 2006 Laser-plasma acceleration of quasi-monoenergetic protons from microstructured targets *Nature* **439** 445–8
[8] Hegelich B M, Albright B J, Cobble J, Flippo K, Letzring S, Paffett M, Ruhl H, Schreiber J, Schulze R K and Fernández J C 2006 Laser acceleration of quasi-monoenergetic MeV ion beams *Nature* **439** 441–4
[9] Ter-Avetisyan S, Schnürer M, Nickles P V, Kalashnikov M, Risse E, Sokollik T, Sandner W, Andreev A and Tikhonchuk V 2006 Quasimonoenergetic deuteron bursts produced by ultraintense laser pulses *Phys. Rev. Lett.* **96** 145006
[10] Fuchs J *et al* 2007 Laser-foil acceleration of high-energy protons in small-scale plasma gradients *Phys. Rev. Lett.* **99** 015002
[11] Mora P 2007 Laser driven ion acceleration *AIP Conf. Proc.* **920** 98–117
[12] Yin L, Albright B J, Hegelich B M, Bowers K J, Flippo K A, Kwan T J T and Fernández J C 2007 Monoenergetic and GeV ion acceleration from the laser breakout afterburner using ultrathin targets *Phys. Plasmas* **14** 056706
[13] Robson L *et al* 2007 Scaling of proton acceleration driven by petawatt-laser–plasma interactions *Nat. Phys.* **3** 58–62
[14] Yin L, Albright B J, Bowers K J, Jung D, Fernández J C and Hegelich B M 2011 Three-dimensional dynamics of breakout afterburner ion acceleration using high-contrast short-pulse laser and nanoscale targets *Phys. Rev. Lett.* **107** 045003
[15] Esirkepov T, Borghesi M, Bulanov S V, Mourou G and Tajima T 2004 Highly efficient relativistic-ion generation in the laser-piston regime *Phys. Rev. Lett.* **92** 175003
[16] Yan X Q, Lin C, Sheng Z M, Guo Z Y, Liu B C, Lu Y R, Fang J X and Chen J E 2008 Generating high-current monoenergetic proton beams by a circularly polarized laser pulse in the phase-stable acceleration regime *Phys. Rev. Lett.* **100** 135003
[17] Liu C S, Tripathi V K and Shao X 2008 Laser acceleration of monoenergetic protons trapped in moving double layer *AIP Conf. Proc.* **1061** 246–54
[18] Klimo O, Psikal J, Limpouch J and Tikhonchuk V T 2008 Monoenergetic ion beams from ultrathin foils irradiated by ultrahigh-contrast circularly polarized laser pulses *Phys. Rev. Spec. Top.—Accel. Beams* **11** 031301
[19] Tripathi V K, Liu C S, Shao X, Eliasson B and Sagdeev R Z 2009 Laser acceleration of monoenergetic protons in a self-organized double layer from thin foil *Plasma Phys. Control Fusion* **51** 024014
[20] Robinson A P L, Zepf M, Kar S, Evans R G and Bellei C 2008 Radiation pressure acceleration of thin foils with circularly polarized laser pulses *New J. Phys.* **10** 013021
[21] Eliasson B, Liu C S, Shao X, Sagdeev R Z and Shukla P K 2009 Laser acceleration of monoenergetic protons via a double layer emerging from an ultra-thin foil *New J. Phys.* **11** 073006
[22] Liu T-C, Shao X, Liu C-S, Su J-J, Eliasson B, Tripathi V, Dudnikova G and Sagdeev R Z 2011 Energetics and energy scaling of quasi-monoenergetic protons in laser radiation pressure acceleration *Phys. Plasmas* **18** 123105
[23] He M-Q, Shao X, Liu C-S, Liu T-C, Su J-J, Dudnikova G, Sagdeev R Z and Sheng Z-M 2012 Quasi-monoenergetic protons accelerated by laser radiation pressure and shocks in thin gaseous targets *Phys. Plasmas* **19** 073116
[24] Henig A *et al* 2009 Radiation-pressure acceleration of ion beams driven by circularly polarized laser pulses *Phys. Rev. Lett.* **103** 245003
[25] Palmer C A J *et al* 2012 Rayleigh–Taylor instability of an ultrathin foil accelerated by the radiation pressure of an intense laser *Phys. Rev. Lett.* **108** 225002
[26] Aurand B *et al* 2013 Radiation pressure-assisted acceleration of ions using multi-component foils in high-intensity laser–matter interactions *New J. Phys.* **15** 033031
[27] Pegoraro F and Bulanov S V 2007 Photon bubbles and ion acceleration in a plasma dominated by the radiation pressure of an electromagnetic pulse *Phys. Rev. Lett.* **99** 065002
[28] Liu C S, Shao X, Eliasson B, Liu T C, Dudnikova G and Sagdeev R Z 2011 Laser acceleration of quasi-monoenergetic protons via radiation pressure driven thin foil *AIP Conf. Proc.* **1320** 104–10
[29] Steinke S *et al* 2013 Stable laser-ion acceleration in the light sail regime *Phys. Rev. Spec. Top.—Accel. Beams* **16** 011303

[30] Yu T-P, Pukhov A, Shvets G and Chen M 2010 Stable laser-driven proton beam acceleration from a two-ion species ultrathin foil *Phys. Rev. Lett.* **105** 065002
[31] Kar S *et al* 2012 Ion acceleration in multispecies targets driven by intense laser radiation pressure *Phys. Rev. Lett.* **109** 185006
[32] Liu T-C, Shao X, Liu C-S, He M, Eliasson B, Tripathi V, Su J-J, Wang J and Chen S-H 2013 Generation of quasi-monoenergetic protons from thin multi-ion foils by a combination of laser radiation pressure acceleration and shielded Coulomb repulsion *New J. Phys.* **15** 025026
[33] Liu T-C, Shao X, Liu C-S, Eliasson B, Wang J and Chen S-H 2014 Spot size dependence of laser accelerated protons in thin multi-ion foils *Phys. Plasmas* **21** 063102
[34] Aurand B *et al* 2013 Preparation and characterization of nanometer-thin freestanding polymer foils for laser-ion acceleration *J. Polym. Sci.* B **51** 1355–60
[35] Davison E and Colquhoun W 1985 Ultrathin formvar support films for transmission electron microscopy *J. Electron Microsc. Tech.* **2** 35–43
[36] Braun J, Day P K, Toennies J P, Witte G and Neher E 1997 Micrometer-sized nozzles and skimmers for the production of supersonic He atom beams *Rev. Sci. Instrum.* **68** 3001–9
[37] Haberberger D, Tochitsky S, Fiuza F, Gong C, Fonseca R A, Silva L O, Mori W B and Joshi C 2012 Collisionless shocks in laser-produced plasma generate monoenergetic high-energy proton beams *Nat. Phys.* **8** 95–9
[38] Forslund D W and Freidberg J P 1971 Theory of laminar collisionless shocks *Phys. Rev. Lett.* **27** 1189–92
[39] Eliasson B 2014 Ion shock acceleration by large amplitude slow ion acoustic double layers in laser-produced plasmas *Phys. Plasmas* **21** 023111
[40] Nieter C and Cary J R 2004 VORPAL: a versatile plasma simulation code *J. Comput. Phys.* **196** 448–73